

Probing the ^6He halo structure with elastic and inelastic proton scattering

A. Lagoyannis^{1,2}, F. Auger¹, A. Musumarra^{1*}, N. Alamanos¹, E. C. Pollacco¹, A. Pakou², Y. Blumenfeld³, F. Braga¹, M. La Commara⁴, A. Drouart¹, G. Fioni¹, A. Gillibert¹, E. Khan³, V. Lapoux¹, W. Mittig⁵, S. Ottini-Hustache¹, D. Pierroutsakou⁴, M. Romoli⁴, P. Roussel-Chomaz⁵, M. Sandoli⁴, D. Santonocito^{3,*}, J. A. Scarpaci³, J.L. Sida¹ and T. Suomijärvi³

¹*DSM/DAPNIA CEA SACLAY, 91191 Gif-sur-Yvette, France*

²*Department of Physics, The University of Ioannina, 45110 Ioannina, Greece*

³*Institut de Physique Nucléaire, IN2P3-CNRS, F-91406, Orsay, France*

⁴*University of Napoli and INFN Sezione di Napoli, I-80125, Napoli, Italy*

⁵*GANIL, BP 5027, F-14021, Caen, France*

S. Karataglidis^{6,7} and K. Amos⁸

⁶*TRIUMF, 4004 Wesbrook Mall, Vancouver, British Columbia, V6T 2A3, Canada*

⁷*Theory Division, Los Alamos National Laboratory, Los Alamos, New Mexico, 87545*

⁸*School of Physics, University of Melbourne, Parkville 3052, Victoria, Australia*

(May 20, 2019)

Abstract

Proton elastic scattering and inelastic scattering to the first excited state of ^6He have been measured over a wide angular range using a 40.9A MeV ^6He beam. The data have been analyzed with a fully microscopic model of proton-nucleus scattering using ^6He wave functions generated from large space shell model calculations. The inelastic scattering data show a remarkable sensitivity to the halo structure of ^6He .

PACS number(s): 25.60.-t, 25.40.Cm, 25.40.Ep, 24.10.Ht

Typeset using REVTeX

*present address:INFN-Laboratori Nazionali del Sud, Via S. Sofia 44, 95123 Catania Italy

It is well known that neutron rich weakly bound light nuclei have abnormally large radii [1]. This phenomenon is attributed to the valence neutrons which tunnel out of the core so that they have a large probability to be present at distances greater than the normal nuclear radius. Considerable experimental and theoretical efforts have been devoted to the understanding of the structure of these so-called halo nuclei [2,3]. However, due to the low intensities of the available exotic beams, it is only recently that inelastic scattering and transfer reactions on light particles, which are the best tools to probe deeply the structure of nuclei could be undertaken under good conditions. Experimentally, the Borromean ${}^6\text{He}$ nucleus is the best candidate for this kind of study since the only confirmed discrete state is a 2^+ state situated at 1.87 MeV [4]. It has been investigated through the measurement of interaction, dissociation and elastic scattering cross sections [5]. However, apart from elastic scattering, those reactions involve breakup of the ${}^6\text{He}$ into its constituents (${}^4\text{He} + n + n$), and that has been shown to be significantly influenced by final state interactions [6], which destroys information about the ${}^6\text{He}$ ground state.

To study the microscopic structure of ${}^6\text{He}$ we measured elastic and inelastic scattering of ${}^6\text{He}$ from protons by making use of a new large acceptance detector array MUST [9]. In this letter, extended angular distributions are presented along with a fully microscopic analysis using wave functions generated from large space shell model calculations allowing all the nucleons of ${}^6\text{He}$ to be active in the field. The inelastic scattering angular distribution to the 2^+ state can only be reproduced if wave functions including a neutron halo are used, demonstrating for the first time a strong sensitivity of inelastic scattering data to the halo structure.

The experiment was performed at the GANIL facility with a 40.9A MeV ${}^6\text{He}$ radioactive ion beam produced by fragmentation of a primary 75A MeV ${}^{13}\text{C}$ beam on a 8.45 mm thick C target located in the SISSI device [10]. The secondary beam was purified with a 0.9 mm thick Al degrader situated between the dipoles of the α -spectrometer. The beam intensity on the polypropylene (CH_2)₃ reaction target was 10^5 particles per second with a 2% total contamination of ${}^8\text{Li}$ and ${}^9\text{Be}$. As the beam spot on the target covered 1 cm^2 with a maximum angular divergence of 1° , two X and Y position sensitive detectors, CATS [11], were placed at 155 cm and 27 cm in front of the target as illustrated in Fig. 1. These detectors provided the impact point and the incident angle on the target event by event with a FWHM resolution of 0.55 mm (X), 0.7 mm (Y) and 0.1° .

The recoiling protons were detected in MUST [9], an array of 8 three-stage telescopes 6 cm \times 6 cm each. The first stages consist in double-sided Si-strip detectors (300 μm). They were placed at 15 cm from the target and covered the angular range between 46 and 90° in the laboratory frame. At this distance, the 1 mm wide strips result in an angular resolution of 0.4° in both X and Y directions. Protons of less than 6 MeV were stopped in these detectors and were identified down to 0.5 MeV by measurement of energy versus time of flight (E-TOF). The start of the TOF measurement was given by the passage of the incident particle in one CATS tracking detector and the overall time resolution was 1.2 ns. Protons in the energy range of 6 to 25 MeV were stopped in the second SiLi stage (3 mm) of the telescopes while those in the energy range from 25 to 70 MeV were stopped in the third CsI stage (15 mm). They were identified by the $\Delta E - E$ method.

The ejectile was detected in coincidence with the recoiling proton to suppress the protons emitted from excited nuclei produced in central collisions of ${}^6\text{He}$ on the carbon contained

in the target. The coincidence allowed also to suppress the protons coming from reactions induced by the beam contaminants on the target. The ejectile was detected in a plastic wall, situated at 75 cm behind the target and made up of 6 horizontal bars of BC408, $8 \times 50 \text{ cm}^2$ and 3 cm thick. Each bar was read out by a photo-multiplier at each end. The large angular coverage of the wall was imposed by the in flight decay of ${}^6\text{He}$ (${}^6\text{He} \rightarrow \alpha + 2n$) that occurs for excitation energies higher than the $2n$ separation energy of 0.9 MeV [4]. Identification and counting of the beam particles were achieved in a plastic scintillator with a diameter of 2.8 cm and centered at zero degrees.

To measure angular distributions down to 10° in the center of mass (85° in the laboratory) where the energy of the recoiling protons decreases down to 0.5 MeV, a 1.48 mg/cm^2 thick polypropylene target was used. Good statistics at larger angles was obtained by using a 8.25 mg/cm^2 thick target. Elastic (respectively inelastic) events were extracted by requiring that a proton be detected in coincidence with a ${}^6\text{He}$ (respectively alpha particle). Protons were selected with contours on the E-TOF and $\Delta E - E$ planes of MUST and ${}^6\text{He}$ (alpha particles) with contours on the E-TOF matrix of the plastics. Events corresponding to the excitation of the 2^+ state were extracted from inelastic events by taking a window between 0.8 and 2.3 MeV on the excitation energy spectrum of ${}^6\text{He}$ calculated from the measured proton energy and angle. As an illustration, the excitation energy spectrum of inelastic events measured between 60 and 70° in the laboratory is shown in Fig. 2. A small contamination remains from elastic scattering and the high energy side of the 2^+ peak is contaminated by low lying excitations in the continuum and by the fragmentation processes. In order to estimate the background under the 2^+ peak, for each bin of 2° in the laboratory, the spectrum was fitted with four components as shown in Fig. 2: a small constant background corresponding to the background observed at the left of the elastic peak; two Gaussians for the elastic and inelastic peaks having the same width as the ${}^6\text{He}$ elastic peak; and a third Gaussian on the high energy side to simulate the excitations in the continuum. In order to appreciate the uncertainty on the background subtraction, the fit was also done with a linear component beginning at the $2n$ separation energy (0.9 MeV) instead of the third Gaussian. The background represented between 10 and 30% of the peak depending on the angle with an uncertainty of $\pm 5\%$ on this percentage. Elastic and 2^+ state contributions were extracted for each 1° bin in the laboratory frame and normalized with the acceptance of the detection system, the target thickness ($\pm 5\%$ uncertainty) and the number of incident ${}^6\text{He}$ ($\pm 3\%$ uncertainty).

Angular distributions in the center of mass are presented in Fig. 3. The error bars given for elastic scattering are purely statistical whereas the error bars quoted for the inelastic scattering include in addition the error due to the background subtraction.

Calculations for the elastic proton scattering data were made using a fully microscopic model of the optical potential [12]. In this model, the potential is obtained in coordinate-space by folding a complex energy- and density-dependent effective nucleon-nucleon (NN) interaction with the one-body density-matrix elements (OBDME) and single particle bound states of the target generated by shell model calculations. As the approach accounts for the exchange terms in the scattering process the resulting complex optical potential is non-local. This model has been applied successfully to calculate elastic and inelastic scattering of protons from many stable and unstable nuclei ranging from ${}^3\text{He}$ to ${}^{238}\text{U}$ at different energies between 65 MeV and 300 MeV [13–16]. The effective interaction and the structure details

were all preset and no *a posteriori* adjustment or simplifying approximation was made to the folded optical potentials. Hence the observables obtained are predictions. Hereafter, we refer to the process of making such potentials as g folding.

Calculations of the transition amplitudes for the inelastic scattering have been done within the distorted wave approximation (DWA). The same effective NN interaction and shell model calculations used to make the g folding optical potential have been respectively used for the transition operator and the transition OBDME. For the stable nuclei whose spectroscopy is well defined from the measurement of inelastic electron scattering form factor, the inelastic scattering has been shown to be very sensitive, more than elastic scattering, to the details of the effective interaction [13]. Conversely, when the effective interaction was well established, the analysis of inelastic data turned out to be a very sensitive test of the model structure used for the nucleus [13,14]. As for elastic scattering the calculations were parameter free.

To apply these models to 40 MeV proton scattering, the effective NN interaction had to be determined. As for the higher energies, it has been parametrized as a sum of central, two-body spin orbit and tensor components, each of them being a set of Yukawa functions of various ranges. This specific form is dictated by the structure chosen in the program DWBA98 [17] which has been used for the analysis of both the elastic and inelastic scattering data. The complex, energy- and density-dependent strength and the range of each Yukawa function were obtained by accurately mapping the on- and half-on-shell g matrices which are solutions of the Brueckner-Bethe-Goldstone equations of the Bonn-B [18] realistic NN interaction. The validity of the 40 MeV effective interaction has been verified by calculations of cross sections and analyzing powers of proton elastic scattering for different stable nuclei [19].

With the effective NN interaction set, it remained only to define the structure of ${}^6\text{He}$. A view that this nucleus should resemble an α particle with two extraneous neutrons has fostered a semi-microscopic cluster model treatment of the system [20]. On the other hand, large space (no-core) shell model calculations [21,22] and quantum Monte Carlo calculations [23] which are fully microscopic have been done. The Navrátil and Barrett [21] large space shell model calculations are suited to our scattering analyses. They allowed the 6 nucleons to be active and their shell model interaction was specified as NN G matrix elements [24] generated from the realistic CD-Bonn NN interaction. We used their complete $6\hbar\omega$ wave functions to specify the relevant ground state and $0^+ \rightarrow 2^+$ transition OBDME for ${}^6\text{He}$. To investigate the sensitivity of the analyses on the size of the model space we have also used wave functions from a complete $4\hbar\omega$ shell model [22]. However, in both models the binding energy of the last neutron is larger than the experimental separation energy 1.87 MeV [4]. That would indicate that the size of the model spaces used is still too small to give the correct asymptotic behavior of the neutron density.

The $p-{}^6\text{He}$ g folding optical potential made with the shell model prescribed HO functions is almost phase shift equivalent to that obtained using WS functions which allow to fit electron scattering for form factor of ${}^6\text{Li}$ [14]. This led us to use these WS functions but in order to specify the neutron halo in ${}^6\text{He}$ we changed the bound state WS potential so that the 0p-shell binding energy became 2 MeV which is close to the single neutron separation energy. Also the binding energies of the higher orbits were all set to 0.5 MeV as more exact (smaller) values will not influence noticeably results of the scattering. The optical potential

obtained using these adjusted WS single particle wave functions leads to the cross section hereafter designated as *halo*. The use of the HO single particle wave functions given by either shell model leads to the cross section that is designated as *no halo*. Use of the WS wave functions has been shown to reproduce the r.m.s. radius of ${}^6\text{He}$ [22].

The elastic scattering data are compared in Fig. 3(a) to the halo (solid line) and no halo (dashed line) calculations. The two calculations are very similar up to 60° and notably differ at larger angles. The agreement of the calculations with the data is very good up to 60° . The few data beyond these angles are better reproduced by the halo description but it is clear that data at larger momentum transfers are required to use elastic scattering as a probe of the halo structure of ${}^6\text{He}$.

The very good agreement obtained with the elastic scattering data is essential since it validates the g folding optical potential used to define the distorted waves in the DWA analysis of the inelastic scattering leading to the $2^+; T = 1$ state. Halo (solid line) and no halo (dashed line) calculated cross sections for the 2^+ state are presented in Fig. 3(b). Contrary to the elastic scattering, the sensitivity to the halo is important over the entire angular domain. The data are very well reproduced by the halo calculation. This conclusion is strengthened by the fact that the results for both elastic and inelastic scattering obtained by using $4\hbar\omega$ [22] rather than $6\hbar\omega$ model space wave functions and also by using the Paris Potential [25] rather than the Bonn-B interaction are very similar. The validity of the models used to predict the present data is corroborated by the very good agreement obtained between the result of the $4\hbar\omega$ model (406 mb) and the measured (426 ± 21 mb) [26] reaction cross section.

In conclusion, we have presented data for the elastic and inelastic (2^+) scattering of ${}^6\text{He}$ from hydrogen at $40.9A$ MeV over a large angular domain (10° to 80°). An excellent prediction of both elastic and inelastic data has been made using a fully microscopic, complex, non-local optical potential based on large basis shell-model calculations of ${}^6\text{He}$ with the incorporation of a neutron halo. On the other hand, we have shown that the 2^+ state scattering data are not reproduced by using the unaltered shell model wave functions which overpredict the binding energy of the valence neutrons and thus do not allow the halo to be formed. The sensitivity of the inelastic scattering data to the structure of ${}^6\text{He}$ and the success of the coordinate space scattering theories, based upon effective NN interactions used successfully in analyses of proton scattering from stable nuclei, open large perspectives for the study of the microscopic structure of exotic systems.

FIGURES

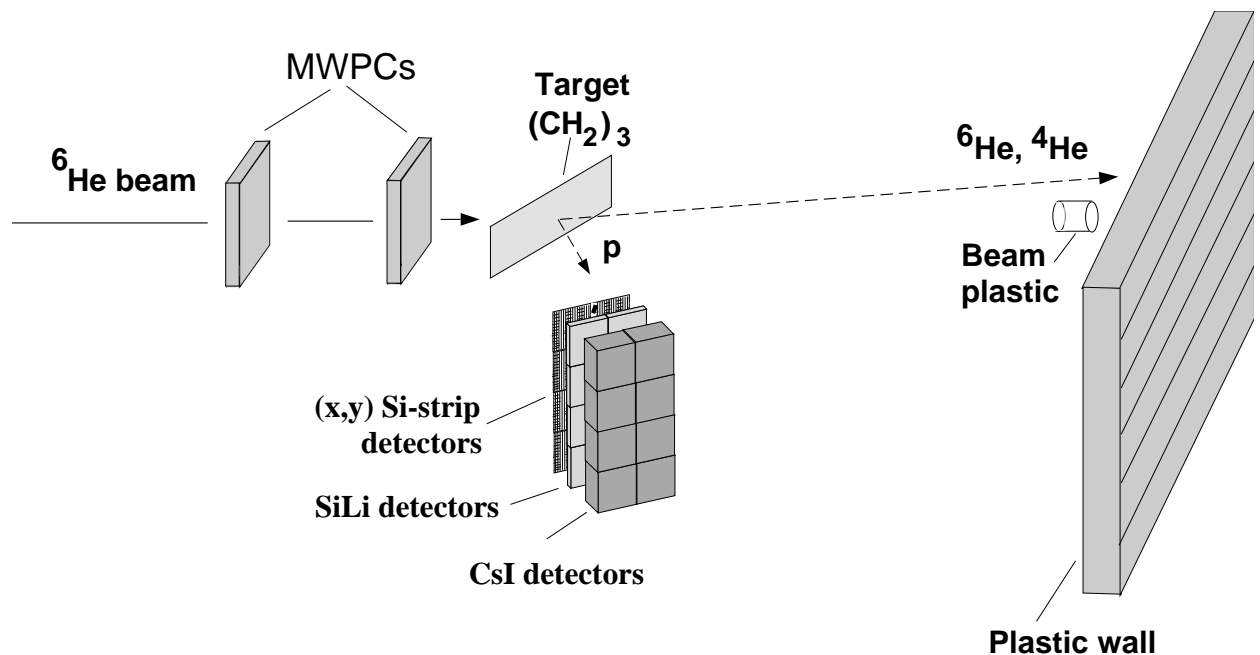


FIG. 1. The experimental set up.

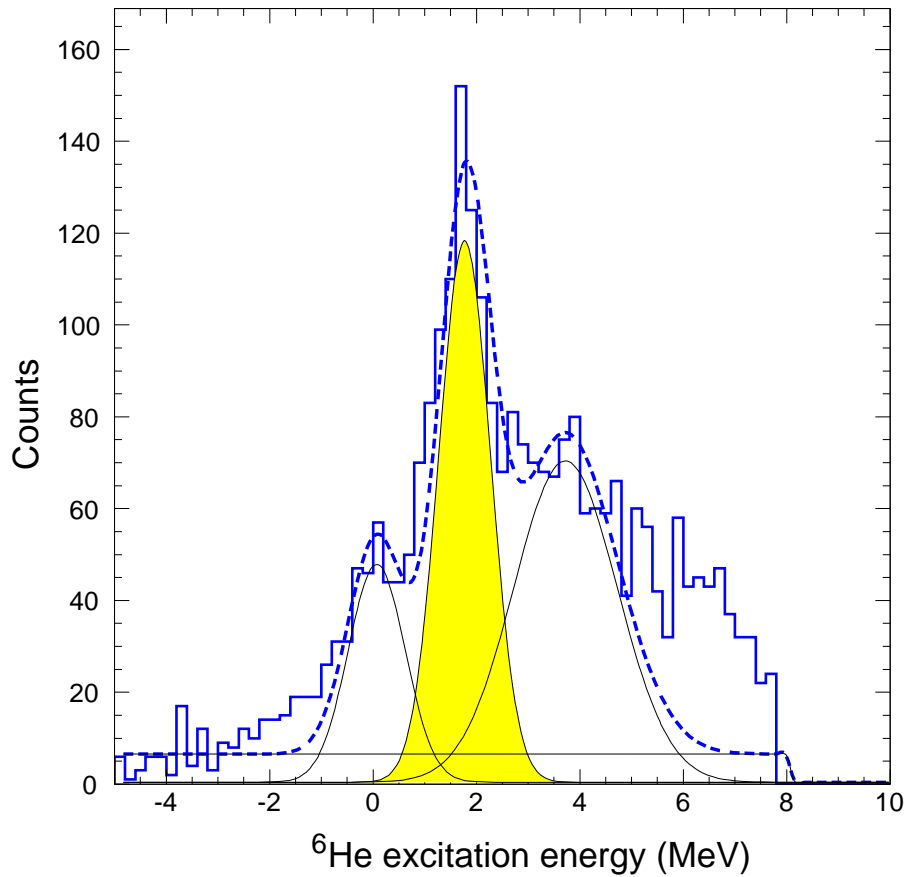


FIG. 2. ${}^6\text{He}$ excitation energy spectrum extracted from protons measured between 60 and 70° in the laboratory in coincidence with an alpha particle. Four components have been considered to estimate the background under the 2^+ peak (see text).

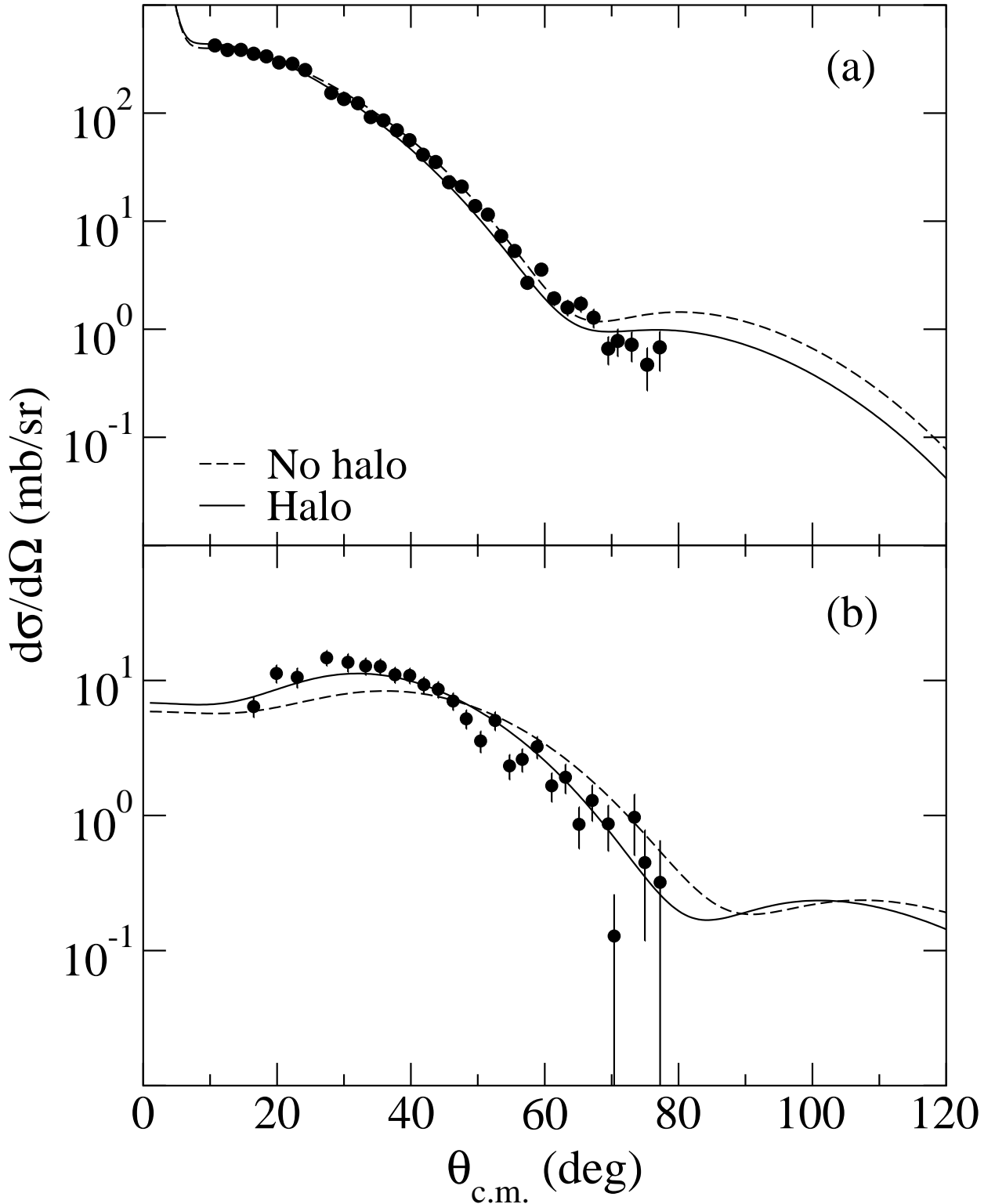


FIG. 3. Differential cross sections for the (a) elastic and (b) inelastic scattering to the of 2^+ state at 1.87 MeV of ${}^6\text{He}$ from hydrogen at $40.9A$ MeV. The present data (circles) are compared to the results of the calculations assuming no halo (dashed line) and halo (solid line) conditions.

REFERENCES

- [1] I. Tanihata, Nucl. Phys. **A478**, 795c (1988).
- [2] P.G.Hansen *et al.*, Ann. Rev. Nucl. Part. Sci **45**, 591 (1995).
- [3] B. Jonson and K. Riisager, Phil. Trans. Roy. Soc. (London) A **356**, 2063 (1998).
- [4] F. Ajzenberg-Selove, Nucl. Phys. **A490**, 1 (1988).
- [5] I. Tanihata *et al.*, Phys. Lett. B **160**, 380 (1985); *ibid.*, Phys. letters B **289**, 261 (1992); J.S. Al-Khalili *et al.*, Phys. Lett. B **378**, 45 (1996); G. D. Alkhasov *et al.*, Phys. Rev. Lett. **78**, 2313 (1997); A. A. Korsheninnikov *et al.*, Nucl. Phys. **A617**, 45 (1997); M.D. Cortina-Gill *et al.*, Nucl. Phys. **A641**, 263 (1998); T. Aumann *et al.*, Phys. Rev. C **59**, 1252 (1999).
- [6] D. Aleksandrov *et al.*, Nucl. Phys. **A633**, 243 (1998).
- [7] H. de Vries *et al.*, At. Data Nucl. Data Tables **36**, 495 (1987).
- [8] A.A. Korsheninnikov and T. Kobayashi, Nucl. Phys. **A567**, 97 (1994).
- [9] Y. Blumenfeld *et al.*, Nucl. Instr. and Meth. A **421**, 471 (1999).
- [10] W. Mittig, Nucl. Phys. News **1**, 30 (1990)
- [11] S. Ottini *et al.*, Nucl. Instr. and Meth. A **431**, 476 (1999).
- [12] P. J. Dortmans and K. Amos, Phys. Rev. C **49**, 1309 (1994).
- [13] S. Karatagliidis *et al.*, Phys. Rev. C **52**, 861, 3224 (1995); *ibid* C **53**, 838 (1996); P. J. Dortmans *et al.*, Phys. Rev. C **57**, 2433 (1998); P. J. Dortmans *et al.*, Phys. Rev. C **58**, 2249 (1998).
- [14] S. Karatagliidis *et al.*, Phys. Rev. C **55**, 2826 (1997).
- [15] P. J. Dortmans *et al.*, J. Phys. G **23**, 183 (1997); Phys. Rev. C **55**, 2723 (1997).
- [16] S. Karatagliidis *et al.*, Phys. Rev. Lett. **79**, 1447 (1997).
- [17] J. Raynal, *Computer code DWBA91*, NEA 1209/02 (1991); K. Amos, University of Melbourne preprint, UM-P-98/63, (1998) (unpublished).
- [18] R. Machleidt *et al.*, Phys. Rep. **149**, 1 (1987).
- [19] P. K. Deb *et al.*, University of Melbourne preprint UM-P-00/10 (2000) submitted for publication to Phys. Rev. C.
- [20] K. Arai *et al.*, Phys. Rev. C **59**, 1432 (1999); and references cited therein.
- [21] P. Navrátil and B. R. Barrett, Phys. Rev. C **54**, 2986 (1996); *ibid* **57**, 3119 (1998).
- [22] S. Karatagliidis *et al.*, Phys. Rev. C **61**, 024319 (2000).
- [23] B.S. Pudliner *et al.*, Phys. Rev. C **56**, 1720 (1997).
- [24] D. C. Zheng *et al.*, Phys. Rev. C **52**, 2488 (1995).
- [25] M. Lacombe *et al.*, Phys. Rev. C **21**, 861 (1980).
- [26] A. de Vismes, P. Roussel-Chomaz, private communication.